Renewable Energy 75 (2015) 37–43

Contents lists available at ScienceDirect

Renewable Energy

journal homepage: www.elsevier.com/locate/renene

An aerodynamic analysis of a novel small wind turbine based on impulse turbine principles

Pei Ying, Yong Kang Chen*, Yi Geng Xu

School of Engineering and Technology, University of Hertfordshire, Hatfield, Herts AL10 9AB, UK

ARTICLE INFO

Article history:
Received 4 November 2013
Accepted 18 September 2014
Available online

Keywords:
Wind energy
CFD
Wind tunnel test
Impulse wind turbine
Power coefficient

ABSTRACT

The paper presents both a numerical and an experimental approach to study the air flow characteristics of a novel small wind turbine and to predict its performance. The turbine model was generated based on impulse turbine principles in order to be employed in an omni-flow wind energy system in urban areas. The results have shown that the maximum flow velocity behind the stator can be increased by 20% because of a nozzle cascade from the stator geometry. It was also observed that a wind turbine with a 0.3 m rotor diameter achieved the maximum power coefficient of 0.17 at the tip speed ratio of 0.6 under the wind velocity of 8.2 m/s. It was also found that the power coefficient was linked to the hub-to-tip ratio and reached its maximum value when the hub-to-tip ratio was 0.45. It is evident that this new wind turbine has the potential for low working noise and good starting feature compared with a conventional horizontal axis wind turbine.

© 2014 Elsevier Ltd. All rights reserved.

1. Introduction

Due to the limitation of fossil fuels and concerns over global warming, the wind energy technology has been developed greatly and become one of the mature technologies in the renewable energy field. Wind turbines as wind energy conversion devices can be divided into four categories by the rotor diameter [1]: i) micro-scale (rotor diameter < 0.1 m); ii) small-scale (0.1 m < rotor diameter < 1 m); iii) middle-scale (1 m < rotor diameter < 5 m) and iv) large-scale (rotor diameter > 5 m). Small scale wind turbines have recently become attractive satisfying on-grid and off-grid applications [2]. In an urban area small scale wind turbines can be suitably constructed on the top of a building and could provide electricity directly to the building [3]. In urban areas, the wind velocity on the top of a building is higher than that near the ground. Rich wind energy can compensate electricity consumption of high buildings with wind turbines for both economic and environmental protection purposes. Limited by the rotor diameter, the power coefficient (C_P) of a small scale horizontal axis wind turbine (HAWT) is normally about 0.25 which is lower than that of a large-scale HAWT of over 0.45 [4]. Kishore [5] compared fourteen small-to-middle scale HAWTs with the rotor diameter range from 0.234 m to 2 m and found that the minimum and maximum values of overall efficiency were about 12% and 26%. It appears that this range also applies to vertical axis wind turbines (VAWTs). Pope [6] gave a prediction about power coefficients of Savonius and Zephyr VAWTs and reported that a Savonius turbine with 2 m rotor diameter had the maximum C_P of 0.18 and another one with 1.524 m rotor diameter only managed the maximum C_P of 0.11. Howell [7] studied power performances of a Darrieus VAWT with a straight blade of 0.6 m diameter and reported that the maximum C_P was about 0.2.

An omni-flow wind energy system for urban areas has been developed [8,9]. The shrouds and chambers of this wind energy system can take the entrance wind from different directions and convert the flow to a vertical exit where the turbine is located. The flow velocity at the outlet is increased during this process. However, due to structure features, the flow velocity distribution in front of a turbine blade is not uniform and the blade will experience four to five different flow velocities and the aerodynamic loads during one cycle of revolution [8]. Therefore a wind turbine with the conventional thin blades has difficulty to accommodate the flow conditions in the omni-flow wind energy system. A new type of wind turbine blade is needed.

It has been reported that an impulse turbine has a potential to operate well under the variable air flow velocities in the marine energy field [10,11]. Impulse turbines have been applied in an oscillating water column (OWC) for wave energy conversion [12,13]. In wave energy, the impulse turbine has been proven as the best one in power generation, starting capability and so on [14]. Considering these features, the impulse turbine principles appear

* Corresponding author.
E-mail address: y.k.chen@herts.ac.uk (Y.K. Chen).

http://dx.doi.org/10.1016/j.renene.2014.09.035
0960-1481/© 2014 Elsevier Ltd. All rights reserved.

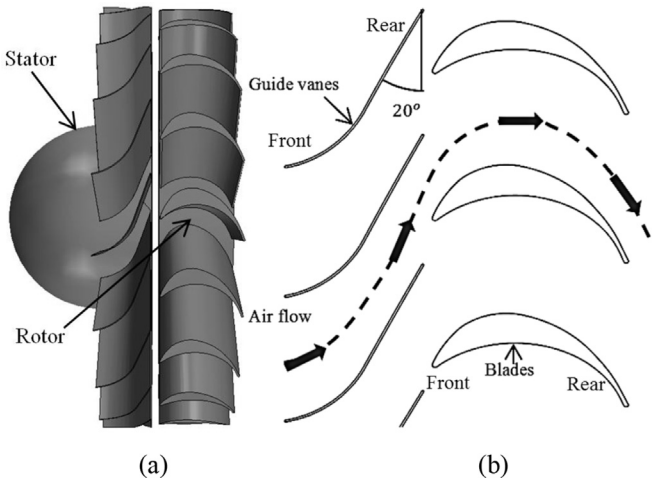

Fig. 1. (a) 3D view of the turbine model and (b) schematic view of guide vanes and blades.

attractive for an omni-flow wind energy system. However, there is little information on impulse turbine principles applied to a wind turbine.

In this paper, a model of a new wind turbine based on impulse turbine principles was presented. Both the experimental and computational investigations were carried out for the aerodynamic properties of a wind turbine under steady velocity wind. The effects of different parameters on the power coefficients and the other properties of this wind turbine were investigated.

2. The turbine model

As shown in Fig. 1, a newly designed wind turbine consists of two parts: a stator with guide vanes and a rotor with blades. This wind turbine was located inside an exit chamber of an omni-flow wind energy system [8]. Fig. 1(a) shows the 3-D model of the turbine generated with CATIA, a Computer Aided Design (CAD) software package. Fig. 1(b) is a schematic view of guide vanes and blades. The guide vanes on the stator led wind to the rotor. Their setting angle was 20°. These guide vanes had thin plate geometry and were fixed on the surrounded wall of the exit chamber. The front part of the guide vane took the shape of an arc and the rear part was straight.

A type of the aerofoil from a unidirectional impulse turbine was employed for the blades on the rotor since this type of blade aerofoil had the best power performance compared with the other blade aerofoils in wave energy [15]. Based upon the sketch from Maeda et al. [16], a further change of the blade aerofoil has been made. The amount of this aerofoil camber takes a 36% of the chord length and it is greater than 4–6% of NACA aerofoils which have been widely used on the wind turbine blades.

3. Experimental apparatus

All lab tests were carried out in a closed return wind tunnel in the School of Engineering and Technology at the University of Hertfordshire. The tunnel had a test section of 1.14 m (width) × 0.84 m (height), with a maximum wind velocity of 25 m/s. A wind turbine test rig was located at the centre of the test section within the tunnel. Fig. 2(a) shows the photograph of the stator with 20 guide vanes inside a cylindrical flow chamber. This wind turbine was produced by rapid manufacturing technology with ABS plastics. As shown in Fig. 2(b), it had 20 blades with a rotor diameter of 300 mm. The hub diameter of this turbine was 135 mm. Both stator and rotor had an identical hub diameter. The hub-tip-speed ratio was 0.45 which was defined as the ratio between the hub diameter and rotor diameter. In this study the dimensionless hub-to-tip ratio was used to represent the hub diameter for a wind turbine. This wind turbine was installed inside a 200 mm long cylinder chamber and the thickness of this chamber was 12 mm. The guide vanes were fixed on the chamber wall. There was a clearance of 2 mm between the blade tip and wall.

Fig. 3 shows the wind turbine test rig together with its primary measurement system utilised in this study. A torque transducer was employed to measure the shaft torque from 0 to 10 Nm with an accuracy of 0.1% and its maximum rotational speed was 5000 rpm. A DC motor was connected to the other end of this torque transducer through a pair of gears to apply a load. The applied load was adjusted by changing the current in the motor. In all tests, an energy loss caused by the bearing and gears was considered. Both Pitot-tube and pressure meter were used to measure both flow pressure and velocity at the selected positions in the wind tunnel test section.

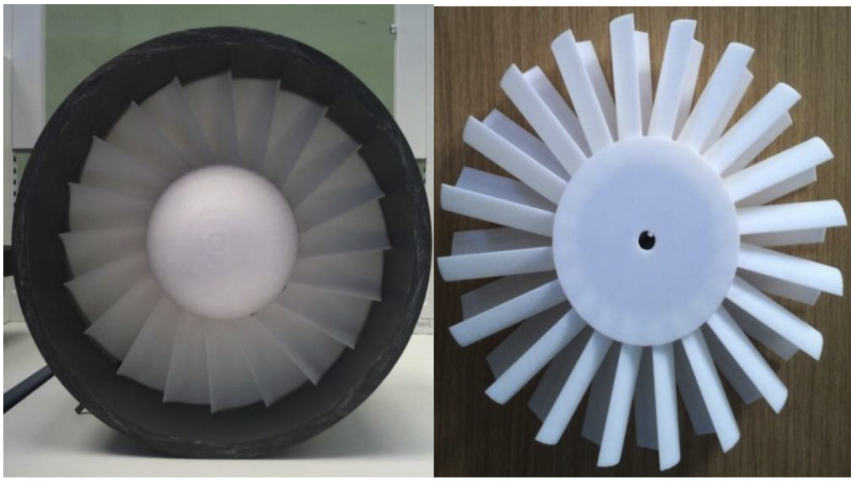

Fig. 2. The wind turbine prototype produced by rapid manufacturing technology: (a) the stator with 20 guide vanes inside a cylinder flow chamber; (b) the rotor with 20 blades.

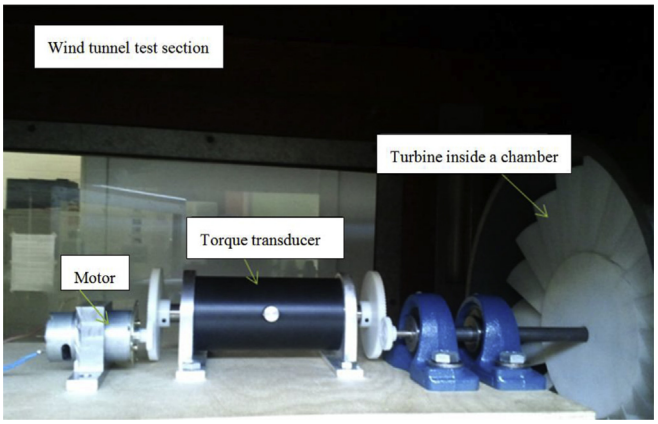

Fig. 3. Test rig within the wind tunnel test section.

4. A computational model

A series of computational fluid dynamics (CFD) simulations for this wind turbine were carried with STAR-CCM+, a CFD software package. Fig. 4 shows a schematic view of the computational domain and the position of the wind turbine model inside the domain. The computational wind turbine model had the same dimensions as the experimental prototype shown in Fig. 2. The test domain was 16 times as long as the length (L) of the chamber in the axial direction, and both the domain width and height were 20 times as long as the rotor diameters (D) of the wind turbine respectively. Both velocity inlet and pressure outlet boundaries were defined as shown in Fig. 4. A uniform wind speed profile was specified at the entrance of this domain. The rotor part of this wind turbine was inside a separated region with a moving reference frame which included the rotating speed and axial definition. The slip conditions were assigned on both the top and bottom boundaries.

Polyhedral grids were employed for the complex geometries of the turbine as shown in Fig. 5. Thin layer grids were employed to surround guide vanes surfaces and blades surfaces. Six different grid numbers were studied in order to check the grid dependency of results. As seen in Fig. 6, when the grid number exceeded about 6,000,000, the difference between the results with various grid numbers was less than 0.1%. Thus it was assumed that the effect of the grid dependency was too small to be considered when the grid number was over 6,000,000. Steady solution and the Reynolds Averaged Navier–Stokes (RANS) equations with Realizable K-Epsilon turbulence model were chosen. A broadband noise source model with Efowcs Williams–Hawkings equations was added into the simulations to estimate the noise distribution around the wind

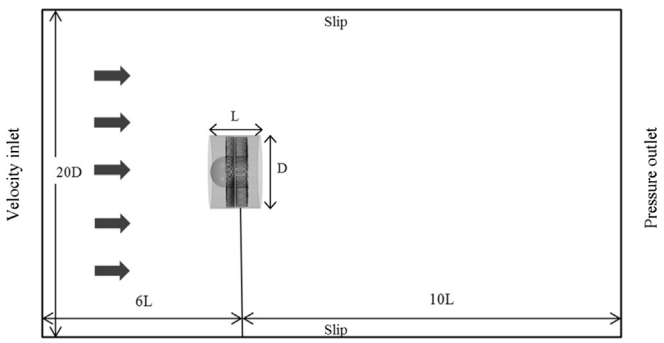

Fig. 4. Schematic view of the domain setup in simulations.

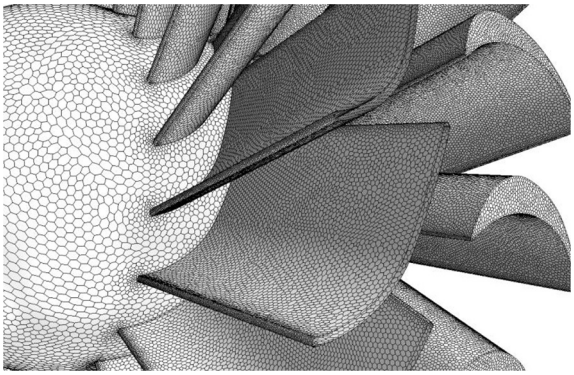

Fig. 5. A part of meshed wind turbine model with polyhedral cells.

turbine with reasonable results in this numerical approach [17]. Residuals in all simulations in this study were lower than 1E-4 after 1600 iterations.

5. Results

5.1. The effect of guide vanes on the passing air flow

Fig. 7(a) shows a group of selected test points near the rear of a guide vane. At each point a radius from the centre of the rotor was employed to define its position on the guide vane as shown in Fig. 7(a). Fig. 7(b) presents the wind speed ratios obtained at the selected test points by both CFD simulations and wind tunnel tests when free-stream wind velocity was 5 m/s.

Wind speed ratio was used to estimate the velocity change and was defined by u/U, where u was wind velocity at a select position and U was the free-stream wind velocity. As shown in Fig. 7(b), the results from both lab tests and computational simulations correlated well. The discrepancies could be caused by the surface roughness and error about the test position. It is evident that the value of most wind speed ratios was greater than 1 except at points close to the chamber wall. The value of maximum wind velocity ratio was about 1.2 at a radius of 90 mm. Wind velocity ratio exceeded 1.1 on points from the radius of 70 mm–112.5 mm (occupies about 28% of the guide vane radius) but was greater than 1 on points from the radius of 70 mm–132.5 mm (which occupies about 42% of the guide vane radius).

Fig. 8(a) shows a schematic view of the flow passage between two guide vanes and the selected test points on the centre line. From the entrance to the exit of the flow passage, the cross area of the flow passage decreased continuously (the entrance area of flow

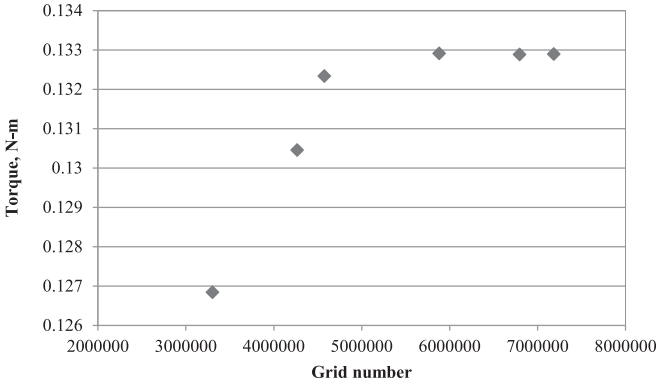

Fig. 6. Torque values under different grid numbers.

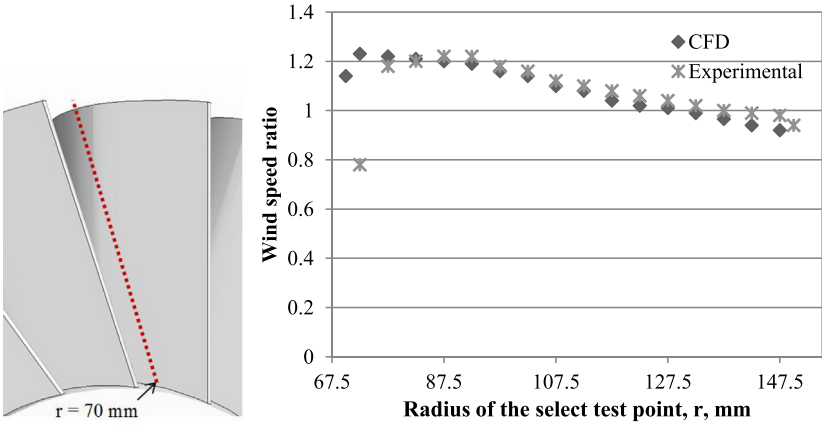

Fig. 7. Wind speed ratios near the rear of a guide vane: (a) selected test points near the rear of a guide vane; (b) wind speed ratios versus selected positions.

passage, A1 > the exit area of flow passage, A2) and it acted as a nozzle cascade. Fig. 8(b) presents velocity and pressure distributions on the centre line of the flow passage at a selected radius of 0.1 m. These results were obtained from the CFD simulations, when the velocity of the free-stream wind was 5 m/s. It can be seen that at the entrance of the flow passage, the air flow had the highest pressure and lowest velocity. Due to the influence of the nozzle cascade the air flow pressure continued to reduce. By contrast, the flow velocity continued to increase as shown in Fig. 8(b). The highest flow velocity was about 5.8 m/s at the exit of the flow passage. Where the distance was less than 15 mm from the entrance of the flow passage, the flow velocity changed slowly. From a distance of 15 mm–30 mm both the flow velocity and the pressure had their changes with large slopes due to a sharp reduction of the cross area of the flow passage. Beyond a distance of 30 mm the air flow left the guide vanes and the flow direction was changed which was decided by the setting angle of guide vanes.

5.2. The key properties of the wind turbine

Two parameters, the power coefficient and torque coefficient, are essential to validate the performance of a wind turbine. Generally, the power coefficient is used to estimate the capability of power generation for a wind turbine and is defined as the ratio of the shaft power from the wind turbine to the power available from the wind [18]:

$$C_P = T\omega/\left(0.5\rho U^3 \pi R^2\right) \tag{1}$$

where T is shaft torque, ω is rotational angular speed, ρ is air density, and R is rotor radius. It is well known that the power is proportional to the square of the rotor radius and cube of the free-stream wind velocity. The tip speed ratio (λ) of the wind turbine is defined as the ratio between the blade tip velocity and free-stream wind velocity,

$$\lambda = V/U = \omega R/U \tag{2}$$

where V is the blade tip velocity.

In the wind tunnel tests, both torques and rotational speeds of the small wind turbine were obtained under various wind velocities. The relationship between the power coefficient and λ is shown in Fig. 9 where the vertical bars represent the experimental scatters. It can be seen that the power coefficient increased with λ

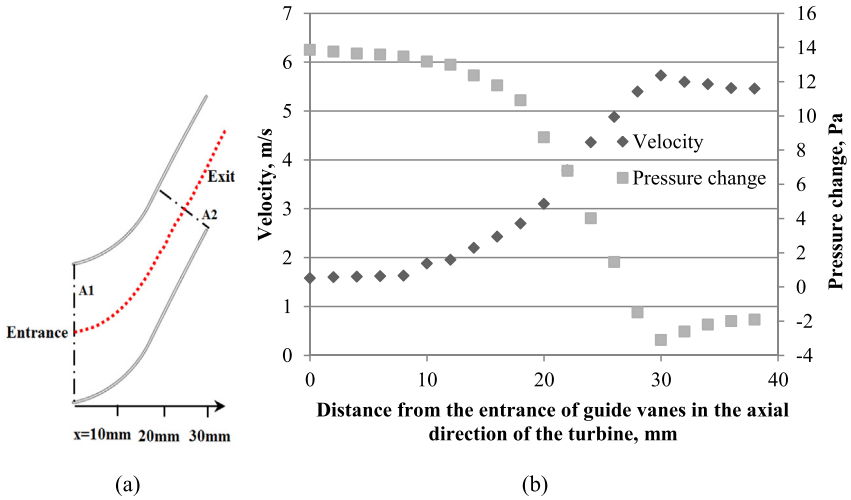

Fig. 8. Distribution of the flow velocity and the pressure change along the centre line of the flow passage: (a) schematic view of the flow passage between two guide vanes; (b) flow velocity and pressure change along the centre line of the flow passage at $r = 100$ mm.

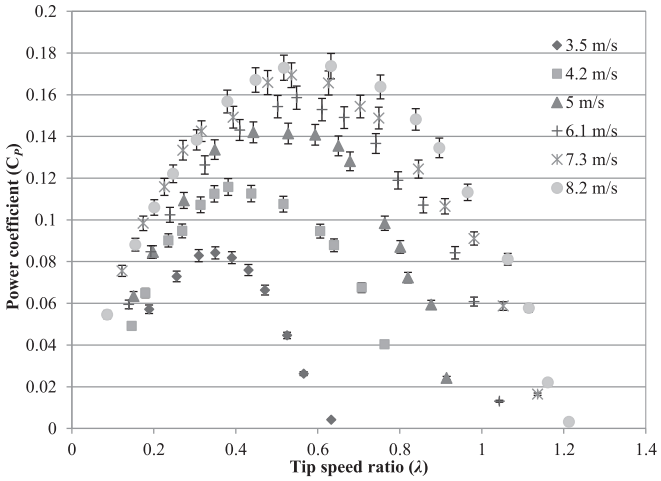

Fig. 9. Power coefficient versus tip speed ratio under various wind velocities.

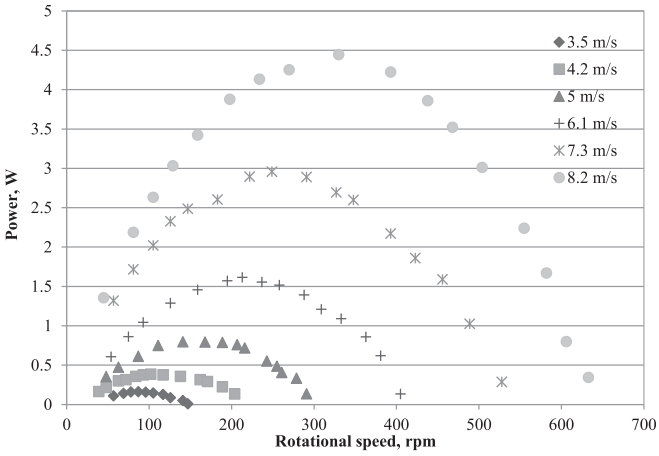

Fig. 11. Relationship between the mechanical power and rotational speed under various wind velocities.

until a maximum value at the middle of λ range and then it decreased and finally became zero when the turbine attained its constant maximum rotational speed. As shown in Fig. 9, with an increase of the entry wind velocity from 3.5 m/s to 8.2 m/s, the maximum power coefficient was increased from about 0.08 to 0.17. Above a wind velocity of 5 m/s, the maximum power coefficients lay in the range of 0.14–0.17 and the optimum tip speed ratios were in the range of 0.5–0.6.

Torque coefficient (C_T) was used to assess the mechanical torque generated by the wind turbine. Wind turbines with higher value of C_T could start and work at lower wind velocity [5]. Torque coefficient is defined as [19]

$$C_T = T/0.5\rho U^2 \pi R^3 \tag{3}$$

Fig. 10 shows the relationship between a torque coefficient and a tip speed ratio. It can be seen that the $C_T - \lambda$ curves are nearly linear. When the wind turbine was stationary, the maximum torque coefficient was obtained. The torque coefficient achieved the maximum value of 0.7 and then decreased to zero gradually. Similar to the power coefficients, a larger torque coefficient was obtained with the higher wind velocity.

Fig. 11 shows the relationship between mechanical power and rotational speed of the shaft. Mechanical power is defined as $P = T\omega$. It can be seen clearly that the higher wind velocities result in the greater power. This wind turbine generated 1.5 W at a wind velocity of 6 m/s. Power was increased to 4.5 W at a wind velocity of 8.2 m/s. The maximum power occurred at a half of the maximum rotational speeds, such as 4.5 W at 350 rpm. With the wind velocity increasing, the rotational speed corresponding to the maximum power output was increased from 80 rpm to 350 rpm.

5.3. The effect of wind turbine hub-to-tip ratio

The effect of a large hub-to-tip ratio on the power coefficient was investigated. A wind turbine model with 0.45 hub-to-tip ratio was simulated at a high wind velocity of 8.2 m/s and the computational results were compared with the experimental results as shown in Fig. 12 in which the vertical bars represent the experimental scatters. It is suggested that the results from both methods are correlated well in trends. The difference between experimental and computational results could be caused by the wind tunnel blockage effect and mechanical friction of the rig in the wind tunnel.

Fig. 13 shows the values of the power coefficients from the wind turbine with different hub-to-tip ratios under the same domain and conditions. $C_P - \lambda$ curves under the three hub-to-tip ratios, 0.35, 0.45 and 0.6, were compared. It can be seen that the wind turbine with 0.45 hub-to-tip ratio has the best values of power coefficient.

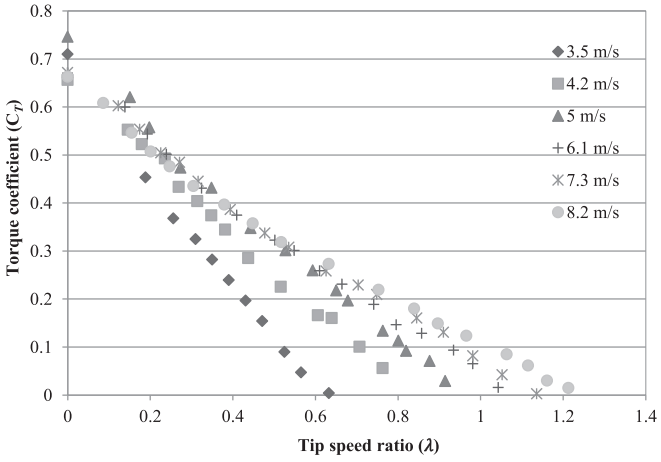

Fig. 10. Torque coefficient against tip speed ratio under various wind velocities.

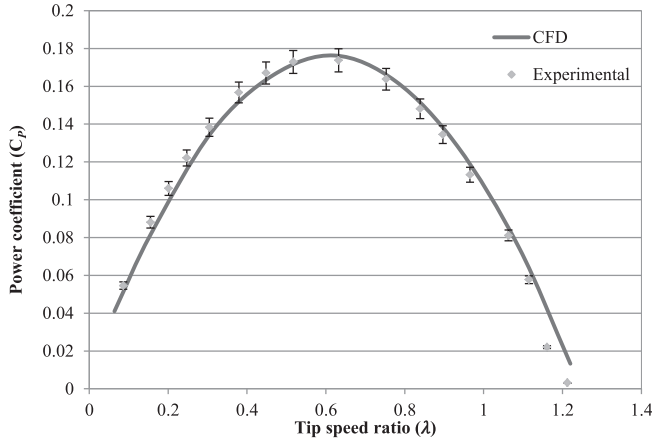

Fig. 12. Comparison of power coefficients from tests and CFD simulations at $U = 8.2$ m/s.

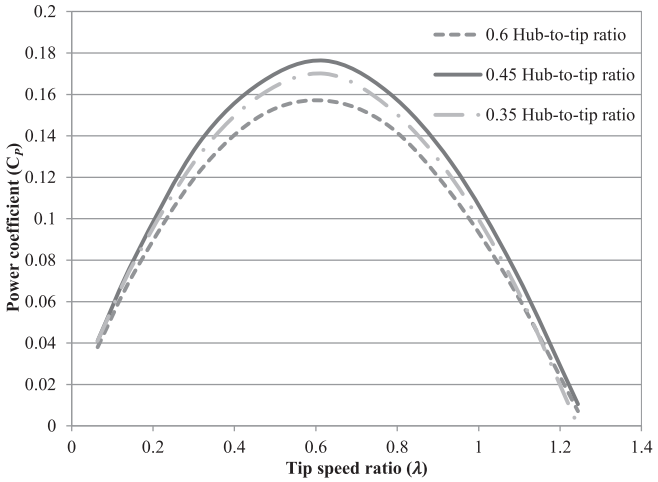

Fig. 13. Comparison of power coefficients under three hub-to-tip ratios at $U = 8.2$ m/s.

There was an increase of 12% in the maximum power coefficient of the turbine with the hub-to-tip ratio of 0.45, compared with that with the hub-to-tip ratio of 0.6. Of the three ratios, the optimal tip speed ratios for the wind turbine were 0.6 and the maximum values were about 1.25.

6. Discussion

It is well known that the power of wind is the cube of the wind flow velocity. Therefore, it is one of the key approaches to provide a slight increase of the wind velocity in order to gain much more power. In this study, the stator of this new wind turbine is employed to increase the wind velocity and change the wind direction when the wind flow passes the blades. The results of the study have shown that the stator can increase the free-stream wind velocity up to 1.2 times as great as its original velocity with a reduction of the blade swept area.

As shown in Fig. 9, this wind turbine normally operated at a tip speed ratio between 0 and 1.2 while a general HAWT operates at a tip speed ratio higher than 4 [18]. Due to the definition of the tip speed ratio, $\lambda = V/U$, under the same wind velocity a smaller range of tip speed ratios means that a wind turbine works with lower blade tip velocities. It is suggested that this wind turbine works with lower blade tip velocities compared with general HAWTs. The lower blade tip velocities for a wind turbine are generally associated with lower working noise [20], therefore, it is suggested that this novel wind turbine works with a low noise level. This suggestion is reflected by the simulation results. It was noted in the numerical study that the maximum noise at the blade tip was 49 dB when the wind turbine reached the maximum power coefficient under a wind speed of 8.2 m/s. It was also observed that the noise level was decreased to about 20 dB at 1 m away from the turbine. As shown in Fig. 12, the tip speed ratio varies from 0 to 1.2. It has been observed that the tip speed ratio is also in the same range from 0 to 1.2 at the different number of blades and that the effect of the blade number on the noise is not significant. However, a reduction of blade number from 20 to 15 will decrease the maximum power coefficient up to 20% [21]. It is suggested that a reduction of blade number from 20 has more negative effect on power output but less effect on a noise level.

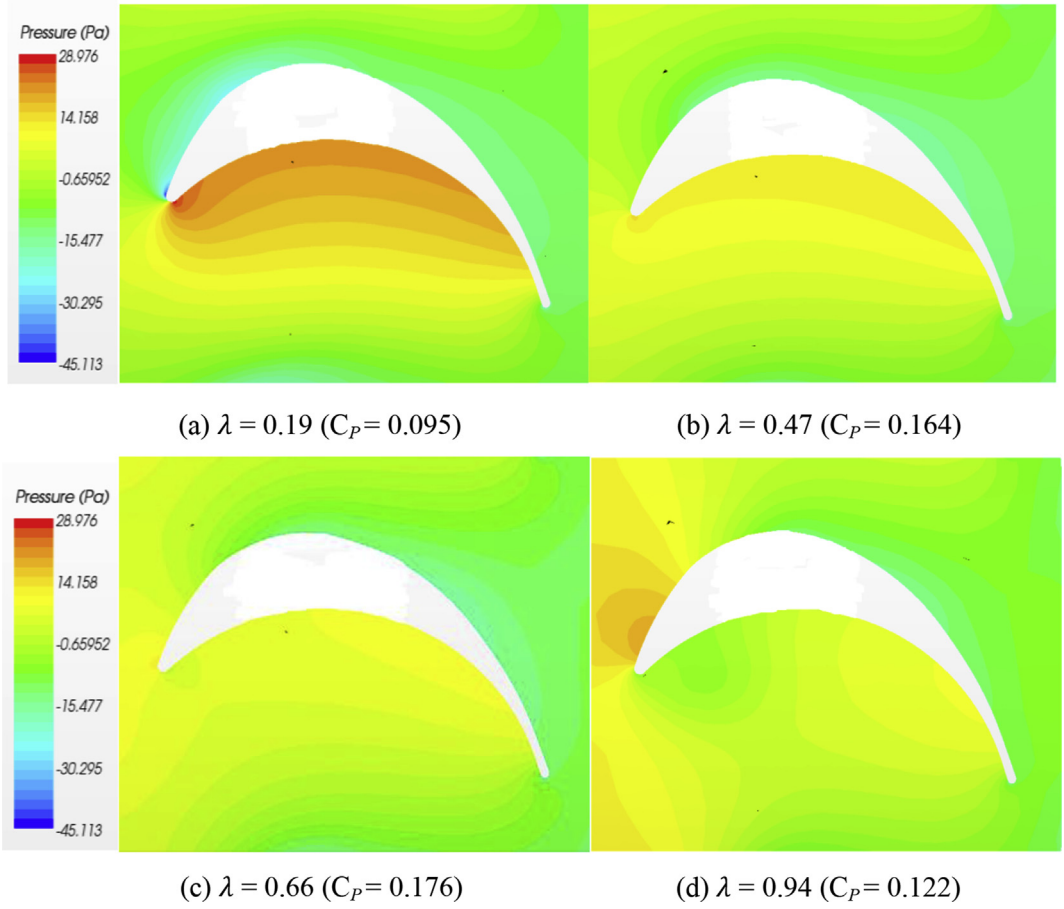

Fig. 14. Pressure distributions around the blade at the radius of 0.13 m under the wind velocity of 8.2 m/s and different tip speed ratios.

As shown in Fig. 10, the maximum torque coefficient C_T is about 0.7 which is greater than that of some HAWTs [5,22,23] when the wind turbine stood still. It is evident that a great torque coefficient allows the wind turbine to start at low wind velocities. Therefore, it is suggested that this novel wind turbine has the potential in good starting capability. The employed aerofoil resulted in good starting capability. Fig. 14 shows pressure distributions around the blade aerofoil. As shown in Fig. 14(a), this blade had the maximum pressure difference at the smallest tip speed ratio. This pressure difference resulted in the aerodynamic forces and led to a great torque coefficient and good starting capability.

With an increase of the tip speed ratios, the pressure difference level decreased as shown in Fig. 14(b, c). With increasing the tip speed ratio to 0.94, the upper surface on the front part of this aerofoil had higher pressure than the lower surface as shown in Fig. 14(d). So, the generated aerodynamic force on the front part hindered the blade rotating and resulted in a reduction of power coefficient as shown in Fig. 9. Therefore, it is feasible to optimise the front part of this aerofoil for better performance on power in future.

In urban areas there are requirements about the noise level and wind has low velocities [24]. It can be seen that this wind turbine has two unique features, the low working noise and good starting capability. This suggests that this wind turbine is suitable to be applied in an urban area.

As shown in Figs. 7 and 12, the comparisons between the CFD results and wind tunnel test results show that the CFD simulations were in good agreement with the experimental measurements. Therefore, it is suggested that the CFD approach in this study can provide reasonable results. One of the advantages using the CFD simulation is that CFD simulation can provide more detailed information and visual indication of flow across the turbine blades, such as the pressure distributions around blades as shown in Fig. 14. It is suggested that this numerical approach can help to understand aerodynamic behaviour of the wind turbine and contribute to the optimisation of this new wind turbine. Typically, with the validated CFD approach, the effect of wind turbine hub-to-tip ratios on power coefficients was studied. Among three compared hub-to-tip ratios, the 0.45 ratio hub has the optimum balance between the wind velocity and the blade swept area to achieve the best value of C_P. The hub with the hub-to-tip ratio of 0.6 limited the blade swept area and reduced the capacity to harvest the available wind energy, even the wind velocity had an increase. On the hub with the hub-to-tip ratio of 0.35 the crowed roots of blades impeded wind flow passing and nearly no torque was generated near the region of blade roots to improve C_P.

7. Conclusions

A new novel small wind turbine based upon the impulse turbine principles has been investigated with both a numerical approach and wind tunnel testing. Based on the above results and discussion, the following conclusions can be drawn:

- It is evident that impulse turbine principles can be employed for an omni-flow wind energy system and an application of the principles has the potentials to improve the performance of this novel wind energy system.
- The employment of a stator with guide vanes has provided a new approach to accelerate the wind velocity of free-stream for the omni-flow wind energy system. The results have showed that the maximum wind velocity behind the stator can be increased up to 1.2 times. Typically, the wind turbine achieved the maximum power coefficient of 0.17 at λ of 0.6 under a wind velocity of 8.2 m/s.
- It is evident that this novel wind turbine has good starting capability and low working noise.
- Hub-to-tip ratio is an important factor in this new wind turbine. This wind turbine of 0.45 hub-to-tip ratio has the best value of power coefficient, C_P.
- With a validation of wind tunnel testing, the CFD simulation, a numerical approach, in this study has provided the acceptable results and this numerical approach can be used in future investigation.

References

[1] Kishore RA, Coudron T, Priya S. Small-scale wind energy portable turbine (SWEPT). J Wind Eng Ind Aerodyn 2013;116:21–31.
[2] Kaldellis JK, Zafirakis D. The wind energy (r)evolution: a short review of a long history. Renew Energy 2011;36:1887–901.
[3] Dayan E. Wind energy in buildings. Refocus 2006;7:33–8.
[4] Singh RK, Ahmed MR. Blade design and performance testing of a small wind turbine rotor for low wind speed applications. Renew Energy 2013;50:812–9.
[5] Kishore RA, Priya S. Design and experimental verification of a high efficiency small wind energy portable turbine (SWEPT). J Wind Eng Ind Aerodyn 2013;118:12–9.
[6] Pope K, Dincer I, Naterer GF. Energy and exergy efficiency comparison of horizontal and vertical axis wind turbines. Renew Energy 2010;35:2102–13.
[7] Howell R, Qin N, Edwards J, Durrani N. Wind tunnel and numerical study of a small vertical axis wind turbine. Renew Energy 2010;35:412–22.
[8] Zhang X, Chen YK, Calay R. Modelling and analysis of a novel wind turbine structure. Int J Model Identif Control 2013;19:142–9.
[9] Sureshan V. Omni-directional wind power station. Patent no. WO2008017106A1; 2008.
[10] Setoguchi T, Santhakumar S, Maeda H, Takao M, Kaneko K. A review of impulse turbines for wave energy conversion. Renew Energy 2001;23:261–92.
[11] Thakker A, Usmani Z, Dhanasekaran TS. Effects of turbine damping on performance of an impulse turbine for wave energy conversion under different sea conditions using numerical simulation techniques. Renew Energy 2004;29:2133–51.
[12] Gomes RPF, Henriques JCC, Gato LMC, Falcão AFO. Multi-point aerodynamic optimization of the rotor blade sections of an axial-flow impulse air turbine for wave energy conversion. Energy 2012;45:570–80.
[13] Falcão AFO. Wave energy utilization: a review of the technologies. Renew Sustain Energy Rev 2010;14:899–918.
[14] Setoguchi T, Takao M. Current status of self rectifying air turbines for wave energy conversion. Energy Convers Manag 2006;47:2382–96.
[15] Jayashankar V, Anand S, Geetha T, Santhakumar S, Jagadeesh KV, Ravindran M, et al. A twin unidirectional impulse turbine topology for OWC based wave energy plants. Renew Energy 2009;34:692–8.
[16] Maeda H, Takao M, Setoguchi T, Kaneko K, Kim TH, Inoue M. Impulse turbine for wave power conversion with air flow rectification system. In: Proceedings of the eleventh international offshore and polar engineering conference, Stavanger, Norway; 2001. p. 646–52.
[17] Tadamasa A, Zangeneh M. Numerical prediction of wind turbine noise. Renew Energy 2011;36:1902–12.
[18] Burton T, Sharpe D, Jenkins N, Bossanyi E. Wind energy handbook. Chichester: John Wiley & Sons, Ltd; 2001.
[19] Duquette MM, Visser KD. Numerical implications of solidity and blade number on rotor performance of horizontal-axis wind turbines. J Sol Energy Eng 2003;125:425–32.
[20] Rogers AL, Manwell JF, Wright S. Wind turbine acoustic noise. Amherst: Renewable Energy Research Laboratory, University of Massachusetts; 2002.
[21] Ying P. Investigation of a novel wind turbine for an omni-flow wind energy system. PhD thesis. UK: University of Hertfordshire; 2014.
[22] Chen TY, Liao YT, Cheng CC. Development of small wind turbines for moving vehicles: effects of flanged diffusers on rotor performance. Exp Therm Fluid Sci 2012;42:136–42.
[23] Ebert PR, Wood DH. Observations of the starting behavior of a small horizontal axis wind turbine. Renew Energy 1997;12:245–57.
[24] Drew DR, Barlow JF, Cockerill TT. Estimating the potential yield of small wind turbines in urban areas: a case study for Greater London, UK. J Wind Eng Ind Aerodyn 2013;115:104–11.